STABILITY ANALYSIS METHODOLOGIES FOR DC POWER DISTRIBUTION SYSTEMS

S.D. Sudhoff, S.F. Glover, S.H. Żak, Purdue University, USA
S.D. Pekarek, University of Missouri – Rolla, USA
E.J Zivi, U.S. Naval Academy, USA
D.E. Delisle, D. Clayton, Naval Sea Systems Command, USA

ABSTRACT

Power electronics based zonal dc power distribution systems are being considered for future Navy ships**.** The stability of dc power electronics based power distribution systems, and in particular dc systems, is a significant design consideration because of the potential for negative impedance induced instabilities. In this paper, methodologies for analyzing the stability of these systems are reviewed. In particular, tools including time-domain simulation, generalized immittance analysis, and polytopic analysis are considered. The use of both time-domain simulation and generalized immittance analysis for a three-zone hardware test system, the Naval Combat Survivability DC Distribution Testbed, is set forth. The predictions of both of these methods are shown to be in agreement with the observed behavior of the system. Polytopic analysis is then considered as a possible future tool for exploring stability properties. The results of each of these analyses as well as the respective advantages and disadvantages of each of the methods are compared.

KEY WORDS

Stability, time-domain simulation, generalized immittance analysis, polytopic models, direct method of Lyapunov

1. INTRODUCTION

Power electronics based power distribution systems are becoming increasingly common, particularly for mobile applications such as aircraft, vehicles, and on future ships. One of the defining characteristics of power electronics based systems is that they facilitate a high degree of automation and nearly instantaneous reconfiguration capabilities. Many power converters also feature nearly perfect regulation of their output objectives. For example, a dc/dc converter module may maintain an essentially constant output voltage regardless of input disturbances. From the output perspective, this property is highly desirable. However, it has unfortunate consequences. In particular, since power electronic converters are very efficient, ideal regulation of the output makes the converter appear as a constant power load from its input side. As such, an increase in input voltage will cause a decrease in input current – and hence the incremental input resistance to such a converter is negative. Negative incremental input resistance is destabilizing – and can result in instability of the interconnected power system. As a result, the stability analysis of such systems is of paramount importance.

In this paper, different methods of analyzing the stability of power electronics based power distribution systems are reviewed and applied to the Naval Combat Survivability DC Distribution System [1], [2], [3]. This hardware testbed consists of ten power converters in a zonal architecture often considered for future Navy ships. Methods of stability analysis are discussed, with special emphasis on time-domain simulation, generalized immittance analysis, and the direct method of Lyapunov. The predictions of the time-domain simulation and the generalized immittance analysis are compared with experimentally measured results. In particular, these two methods are shown to predict the stability (or lack thereof) of the hardware test system. This is the first time the generalized immittance analysis approach has been validated in hardware on a system wide basis. The paper concludes with a discussion of future directions of stability analysis of power electronics based systems using non-linear methods with emphasis on the use of polytopic modeling techniques.

2. STABILITY DEFINITIONS

It is appropriate to begin this paper with definitions of an equilibrium point, an operating point, and of stability. Definitions for these concepts are readily applied to a mathematical model of a system, but are not as readily applied to the system itself since the notion of state variables breaks down when discussing physical systems. Furthermore, even in the case of the mathematical model of a power electronics based system, the state variables in

a model detailed enough to portray the switching action of the power semiconductors will never become constant. Thus when defining terms related to stability it is necessary to differentiate those definitions as applied to a system model from those as applied to the system.

Herein, when referring to a mathematical model, an equilibrium point is a point at which the derivatives of the state variables are zero. In the case of a model in which switching is represented, the equilibrium point is a point at which the fast or dynamic average of the derivatives of the state variables are zero [4]. An operating point is defined as an equilibrium point about which the system is being studied. If conditions are such that there is only one possible equilibrium point then these terms become synonymous. An operating point of the system model is said to be locally stable if, when perturbed from an operating point by a small amount, the system model returns to that operating point. An operating point of the system model is said to be globally stable if the operating point can be perturbed by any amount and still return to that operating point.

In regard to the physical system (as opposed to a mathematical model), an operating point is defined to be the fast average of the voltages and currents that would satisfy power flow requirements for some loading condition. A dc power system is said to be locally stable about an operating point if the system voltages and currents vary only at the forcing frequencies associated with the switching of the power semiconductors and that the average values of these variables is such that all power converters are operating properly. In other words, the system is said to be stable if, neglecting switching induced ripple, the voltages and currents are constant in the steady-state and the level of these voltages and currents is such that all converters are operating in their intended modes of operation. Although this definition is admittedly informal and imprecise, it is nevertheless useful – particularly when we are discussing the stability of the system and not a model of the system.

These comments with regard to stability are intended for informal discussion only. For a thorough and rigorous discussion, the reader is referred to [5] and [6].

3. SYSTEM DESCRIPTION

In order to illustrate the various methods of determining system stability, the Naval Combat Survivability DC Distribution Testbed depicted in Figure 1 is used as an example system. This reduced-scale hardware test bed was developed by the Navy and the Energy Systems Analysis Consortium (ESAC), (a consortium of universities) [7] in order to serve as a resource for researchers in Naval power and propulsion systems. It is intended to play a role analogous to the IEEE test systems for the electric utility grid.

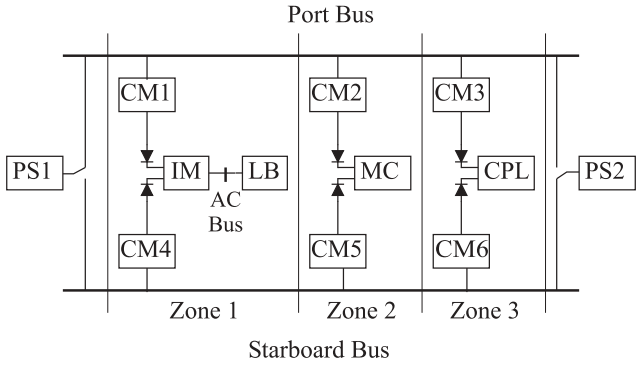

Figure 1. Naval Combat Survivability DC Distribution Testbed.

In this system, there are two power supplies (PS1 and PS2), one of which feeds the port bus, and the other of which feeds the starboard bus (only one connection is active at a time). There are three zones of dc distribution. Each zone is fed by a converter module (CM) on the port bus (CM1, CM2, or CM3) and a converter module on the starboard bus (CM4, CM4, or CM5) operating from one of the two distribution busses. Diodes prevent a fault from one bus being fed by the opposite bus. The converter modules feature a droop characteristic so that they share power. The three loads consist of an inverter module (IM) that in turn feeds an ac load bank (LB), a motor controller (MC), and a generic constant power load (CPL).

Robustness in this system is achieved as follows. First, in the event that either a power supply fails, or a distribution bus is lost, then the other bus will pick up full system load without interruption in service. Faults between the converter module and diode are mitigated by imposing current limits on the converter modules; and again the bus opposite the fault can supply the component. Finally, faults within the components are mitigated through the converter module controls. The result is a highly robust system.

The discussion of the system components begins with the power supply. The power supplies PS1 and PS2 are identical, but have three operating modes. For the studies herein, the uncontrolled rectifier mode is considered. A schematic of the power supply in this mode is depicted in Figure 2. The primary side ac voltage is a nearly ideal 480 V l-l rms source at 60 Hz. The transformer parameters are: primary leakage inductance – 1.05 mH, primary winding resistance – 191 $\mathrm{m}\Omega$, secondary leakage inductance – 1.05 mH, secondary winding resistance - 191 $\mathrm{m}\Omega$, magnetizing inductance – 10.3 H, primary to secondary turns ratio 1.30. All of these parameters apply to the wye-equivalent T-equivalent transformer model and are referred to the primary winding. Finally, the dc link inductance, L_{dc}, is 9.93 mH, the resistance of this inductance, r_{Ldc}, is 273 $\mathrm{m}\Omega$, the dc capacitor, C_{dc}, is 461

mF, and the effective series resistance of the dc capacitor, r_{Cdc}, is 70 mΩ. This capacitor is removed for some studies as noted.

The circuit diagram for the converter modules is depicted in Figure 3. The parameters vary somewhat from converter module to converter module and are listed in Table 1.

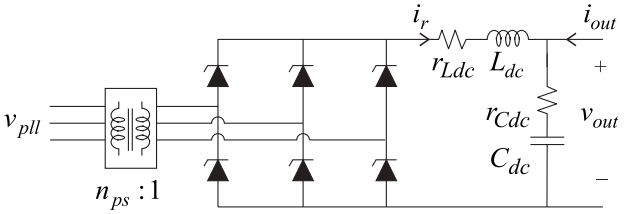

Figure 2. Power supply.

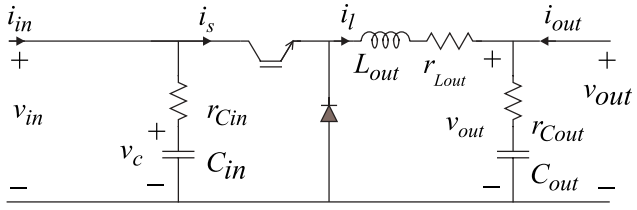

Figure 3. Converter modules circuit diagram.

Table 1. Converter Module Parameters.

	CM1	CM2	CM3	CM4	CM5	CM6
C_{in}, µF	448	461	450	445	450	497
r_{Cin}, mΩ	1080	1070	1080	1080	1090	1070
C_{out}, µF	445	447	448	444	447	491
r_{Cout}, mΩ	70	70	70	70	70	70
r_{Lout}, mΩ	99	102	120	99	97	89

The control of the converter module is depicted in Figure 4. The principal variables not defined by Figure 3 and Figure 4 are the commanded output voltage v_{out}^* and the commanded inductor current i_l^*. This current command, in conjunction with the measured current i_l is used by a hysteresis modulator so that the actual current closely tracks the measured current. The transfer function of the stabilizing feedback $H_{sf}(s)$ is given by

$$H_{sf}(s) = K_{sf}\frac{\tau_{sf1}s}{(\tau_{sf1}s+1)(\tau_{sf2}s+1)} \qquad (1)$$

Parameter values are listed in Table 2.

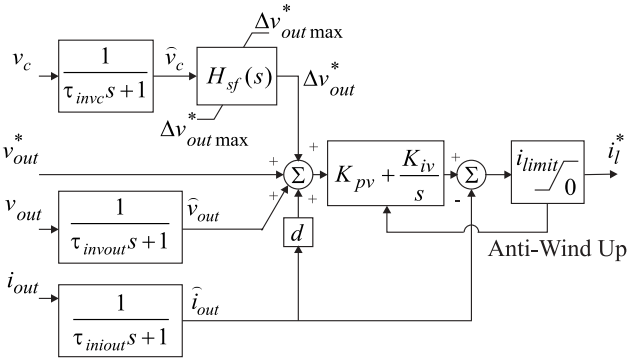

Figure 4. Converter module control.

Table 2. Converter Module Control Parameters.

$\tau_{invc} = 7.96$µs	$\tau_{invout} = 7.96$µs	$\tau_{iniout} = 7.96$µs
$v_{out}^* = 420$ V	$d = 0.8$ A/V	$K_{pv} = 0.628$ AV
$K_{sf} = 0.1$	$\tau_{sf1} = 20$ ms	$\tau_{sf2} = 5$ ms
$\Delta v_{outmax}^* = 20$ V	$i_{limit} = 20$ A	

Because of slight differences in the sensors combined with a fixed-point DSP, the integral voltage gain of the converters varies from converter to converter. The resulting value of K_{iv} for the six converter modules are (in order): 220.6, 218.7, 216.4, 219.6, 219.7, and 218.7 A/Vs.

For the sake of brevity, the inverter module (IM), motor controller (MC), and constant power load (CPL) will not be discussed in detail herein. The salient dynamics of these components may be represented by a capacitor with capacitance C_x and effective series resistance r_x in parallel with an ideal constant power load of P_x. Parameters for this equivalent circuit are listed in Table 3. While this simplistic description can be used to a first approximation a more detailed analysis was used in the actual studies presented. The reader is referred to [1], [2], and [3] for a more detailed description of these components.

Table 3. Load Parameters.

Component	C_x, µF	r_x, mΩ	P_x, kW
IM	590	127	4.69
MC	877	105	2.93
CPL	374	189	5.46

Using this test system, two scenarios are studied. For each case, it is assumed that the starboard bus is out of service due to a fault and that the remainder of the system is being fed from the port power supply. All loads are operating at the capacity listed in Table 3. The difference between the two cases is the system parameters. For Case 1, all parameters are as listed thus far. For Case 2, the power supply output capacitance is removed, and the input capacitance to all the converter modules is reduced to the values listed in Table 4, and, in addition, the stabilizing filter gain, K_{sf}, of all the converter modules are set to zero.

Table 4. Converter Module Parameters For Case 2.

	CM1	CM2	CM3	CM4	CM5	CM6
C_{in}, μF	100	101	102	102	99	103
r_{Cin}, mΩ	226	210	225	204	211	202

4. TIME-DOMAIN SIMULATION

Perhaps the most straightforward means to examine system performance prior to experiment is through the use of time-domain simulation. There are fundamentally two types of simulations that are typically used in this class of systems – so-called 'detailed' model based simulations and non-linear average value model (NLAM) based simulations. The phrase 'detailed' is unfortunate because what is considered detailed is rather arbitrary. In terms of this discussion, however, 'detailed' refers to a simulation in which the switching action of each semiconductor is included, even if only on an 'on' or 'off' basis. Non-linear average value based models refer to simulations where the switching is represented on an average value basis. As a result, state variables are constant in the steady-state (Note that in ac systems, this is still true provided the model is expressed in a synchronous reference frame [4]).

Figure 5 depicts the performance of the test system for the two cases described in the previous section. Variables depicted include:

VPS1	Port bus voltage
VZONE1	Zone 1 voltage (voltage at input to IM)
VZONE2	Zone 2 voltage (voltage at input to MC)
VZONE3	Zone 3 voltage (voltage at input to CPL)

Initially, the parameters are those for Case 1. As can be seen, the waveforms are constant, aside from the switching induced ripple. Approximately one-half of the way into the study, the parameters are changed to match Case 2. It should be observed that this change of parameters does not change the steady-state operating point. It is interesting to observe that the port bus voltage now contains a low-frequency oscillation, which is not related to any of the semiconductor switching frequencies. For this case, the system is predicted to be unstable.

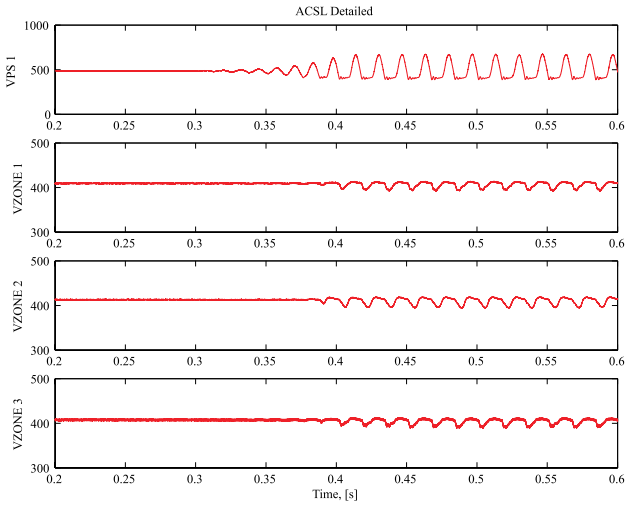

Figure 5. Test system performance, detailed simulation.

In some sense, this study is unrealistic in that the parameters could not be physically changed in the prescribed way. The study is nevertheless useful in that it illustrates both stable and unstable systems with changes that do not affect the steady-state operating point.

The waveforms shown in Figure 5 were obtained using a detailed model based simulation. Figure 6 depicts the waveforms using a NLAM based simulation. The first difference between Figure 5 and Figure 6 is the absence of the switching induced ripple in the waveforms. Otherwise, the simulations are compatible in their predictions, although the exact details of the waveforms vary once the instability has commenced. The reason for this is that models of unstable nonlinear systems tend to exhibit chaotic like behavior – they are extremely sensitive to small differences, for example, in parameters and modeling techniques. The observation that the two models agree well during transients involving stable conditions [8] supports this hypothesis.

Although the conclusions of each time-domain study are similar, there are significant differences between the two time-domain simulations. The NLAM has a computational advantage in that the dynamics are not periodically excited by the switching of the semiconductors. As a results, integration algorithms for stiff systems can be used more effectively than for detailed model simulations. For this system, simulating the 83rd order detailed system model for 0.7 s required 262.3 s of CPU time on a 1 GHz Pentium processor based machine. This time was obtained using the a 5th order Runge-Kutta-Fehlberg integration algorithm with a maximum time step of 10^{-5} s, a minimum time step of 10^{-11} s, and a data logging rate 10^{-4} s. The same study required 55.4 s on the same CPU using the 77th order

NLAM model. In this case Gear's algorithm was used and all other parameters were the same except that the minimum time step was 10^{-15} s.

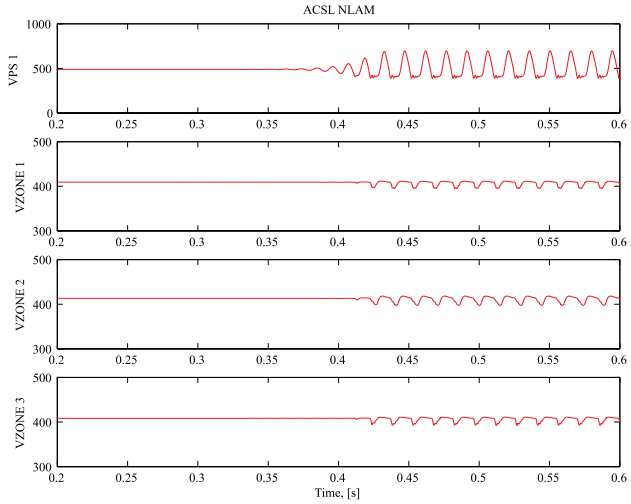

Figure 6. Test system performance, NLAM simulation.

An additional feature of NLAMs is that they can be automatically linearized using many simulation languages including MATLAB [9] and ACSL [10].

As a tool for examining stability, however, the use of time-domain simulation has drawbacks. The primary drawback is that a given study only predicts the stability of a single operating point for a particular perturbation. One valid approach to gain confidence in system behavior is to run massive numbers of studies. However, there is always a possibility that an unstable operating point or scenario can be overlooked.

5. GENERALIZED IMMITTANCE ANALYSIS

For linear systems, the most straightforward alternative to using time domain simulation for examining system stability is to find and inspect the eigenvalues. However, this class of systems is non-linear thereby limiting the usefulness of linear system analysis. One approach can be to simply linearize the system about a given operating point, though such an approach would face the difficulty of needing to check each and every operating point of interest (and there may be infinitely many of them).

An alternative technique, which is also at its roots based in linear system theory is to use the method of generalized immittance analysis [11], [12], [13], and [14]. This is a frequency domain based technique, which has two important characteristics. First, in a single analysis it can be used to test the local stability of all operating points of interest. Second, unlike eigenanalysis, it can be used to set forth design specifications that ensure this condition. For example, in a simple source load system, given a source the method can be used to deduce properties that the load must satisfy in order to ensure the local stability of all operating points of interest.

To illustrate this method, consider the simple source-load system of Figure 7. Let the small-signal impedance characteristic of the source at an operating point x be denoted Z_x, and let the small-signal admittance characteristic of the load be denoted Y_x. Let the set Z represent the generalized impedance and the set Y represent the generalized admittance. Thus, $Z_x \in Z$ and $Y_x \in Y$ for all operating points of interest. The variation of values stems both from nonlinearities as well as parameter uncertainties.

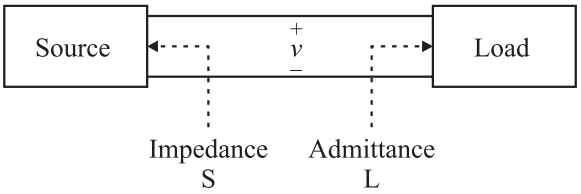

Figure 7. Simple source – load system.

The next step is to select a stability criteria in the s-plane. Figure 8 depicts the ESAC stability criteria with a gain margin GM and phase margin PM. Using generalized admittance analysis, based on a generalized source impedance (load admittance) a load admittance (source impedance) constraint is found such that as long as the generalized load admittance (source impedance) does not intersect the forbidden region then the Nyquist contour of $Z_x Y_x$ will not cross the stability criteria boundary. This in turn ensures that the Nyquist contour of $Z_x Y_x$ cannot encircle –1, which in turn ensures that all operating points considered are locally stable.

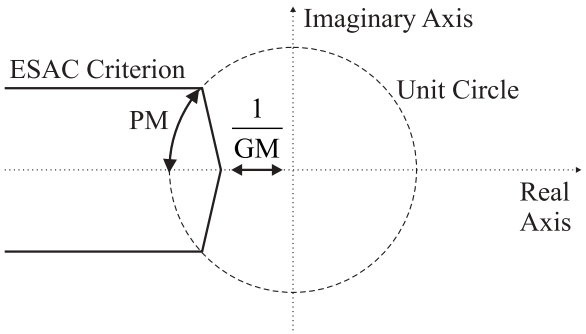

Figure 8. ESAC stability criteria.

The constraint formed is best viewed in the immittance space. To this end, consider Figure 9. The x-axis of this figure is log of frequency, the y-axis is real part in hybrid dB [14], and the z-axis is imaginary part in hybrid dB. The volume to the right is a forbidden region to the load

admittance. The forbidden region is obtained using the stability criteria as well as the generalized source impedance. The volume to the left represents a generalized load admittance.

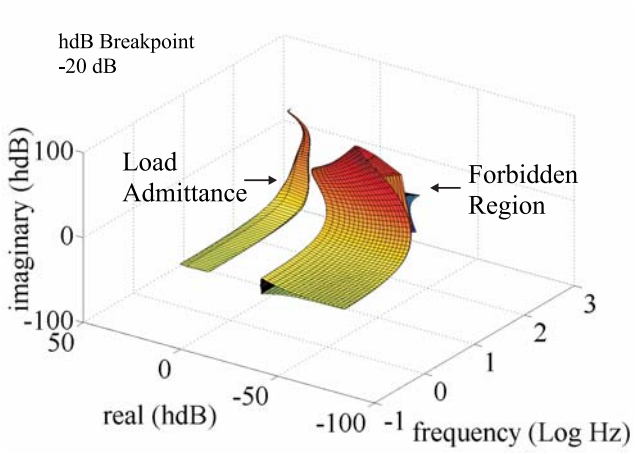

Figure 9. Generalized load admittance and forbidden region for Case 1.

The basic ideas of generalized immittance analysis are set forth in [11], [12], and [13]. These papers primarily concern with simple source-load systems. The extension of the method to large-scale systems is considered in [14]. The first step necessary is to classify the power converters. Single-port converters are classified as S-converters (this category is normally for sources) or L-converters (this category is normally for loads). Two-port converters are classified as H-converters (normally for converters which accept power at one port and supply power to a second port), Y-converters (which are often loads fed by two busses), Z-converters (sources that have two outputs) and C-converter (which are often cables). Formal definitions are set forth in [14]. Once all converters are classified, a series of mapping functions is used to reduce any given system to a source load equivalent. Many possible mapping operations are described in [14]. Often, these mapping operations involve a stability test to ensure that the aggregation of a subset of components is stable.

The steps to analyze the system are illustrated in Figure 10. Figure 10a depicts the original system for Case 1. In this case, CM4, CM5, CM6, and PS are removed from the system because for this scenario the starboard bus is out of service. Consideration of each of the components reveals that PS1 should be classified as an S-converter, CM1, CM2, and CM3 as H-converters, and the IM, MC, and CPL as L-converters. As indicated in Figure 10a, the first operation is three HL-L mappings that result in three aggregate L-converters – CM1-IM, CM2-MC, and CM3-CPL. It should be noted that each of these mappings involves a stability test. In particular, for this mapping to be valid it has to be shown that if CM1 is fed from an ideal source then the system consisting of CM1 and IM is stable. This is done by considering CM1 as a source and IM as a load [14]. The results of this test are not shown due to a lack of space. However, all zones pass this test for all the test cases described in Section 3. The next step is to aggregate the three effective L-converters with a parallel L to L converter mapping as shown in Figure 10b. This results in the system shown in Figure 10c, which consists of a single source and a single effective load. Details on converter types, mapping operations, and an example analysis of other system are set forth in [14].

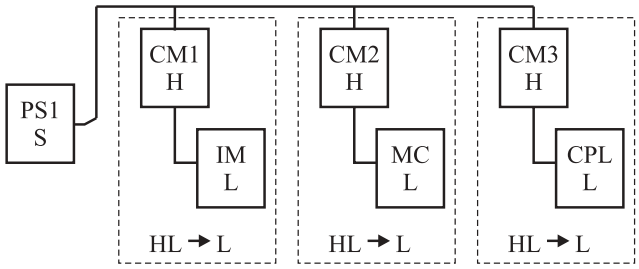

(a). Original System.

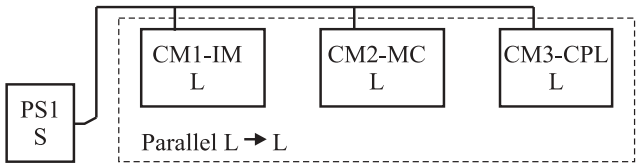

(b). System after simplification.

(c). Final system.

Figure 10. Analysis steps.

Figure 9 depicts the final part of the stability analysis which considers the system of Figure 10c for Case 1. Again, the x-axis is log of frequency, the y-axis is real part of admittance in hybrid dB, and the z-axis is the imaginary part of admittance in hybrid dB. The volume to the right represents a forbidden region for the total system load admittance. The volume to the left represents the generalized load admittance (i.e. set of all possible values of load admittance). As can be seen, the generalized load admittance does not intersect the forbidden region. Thus, local stability (of at least the system model) is guaranteed for all operating points of interest. This is consistent with the results from the time-domain simulations.

Figure 11 depicts the results for Case 2. As can be seen, the generalized load admittance intersects the forbidden region. This does not mean that the actual system is unstable. However, there is no guarantee that the system is stable. From Figure 5 and Figure 6, it is seen that the system model is unstable.

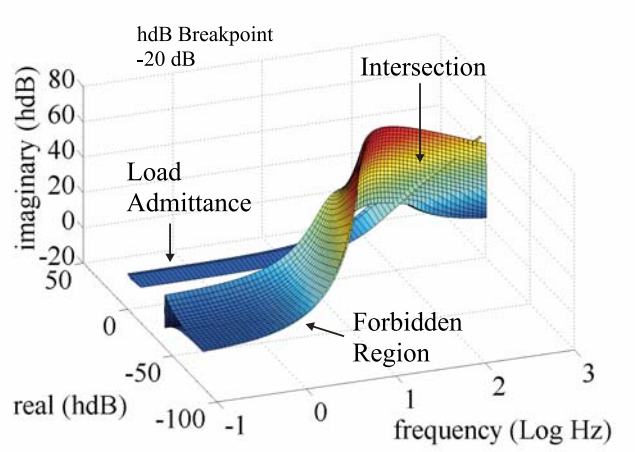

Figure 11. Generalized load admittance and forbidden region for Case 2.

6. EXPERIMENTAL VALIDATION

One of the key measures in evaluating these methods is how well they predict measured performance. Figure 12 and Figure 13 depict the measured time domain performance for Case 1 and Case 2 conditions, respectively. As can seen, all the stability methods consider thus far gave predictions consistent with the observed stability of the system.

7. POLYTOPIC ANALYSIS

In the preceding section, stability analysis of a power electronics based distribution system using time domain simulation and generalized immittance analyses were demonstrated, with excellent results. However, there are shortcomings inherent to either method. In the case of time domain simulation, the results are limited to a very narrow range of conditions. Massive numbers of trajectories must be evaluated to gain confidence in the system performance. In the case of generalized immittance analysis, in some sense a more powerful result is obtained. Using a single analysis, an entire range of operating points can be proven to be locally stable. Furthermore, this approach can be used as a design synthesis tool by providing a method to formulate component specifications. However, the generalized immittance design approach does not guarantee a bounded response in the presence of large disturbances. Hence, there is motivation to perform a stability analysis in which a system can be proven to have an appropriately bounded response to large disturbances.

To this end consider a broad class of nonlinear systems modeled by

$$\dot{\mathbf{x}} = \mathbf{F}(\mathbf{x}, \mathbf{u}) \tag{2}$$

and

$$\mathbf{y} = \mathbf{h}(\mathbf{x}, \mathbf{u}) \tag{3}$$

are considered, where $\mathbf{x} \in \Re^n$ is the state vector, $\mathbf{u} \in \Re^m$ is the input vector, and $\mathbf{y} \in \Re^p$ is the output vector. The above nonlinear model is referred to as the truth model of the underlying system. Systems of this form may be analyzed by the direct method of Lyapunov [5] and [6]. However, there are difficulties associated with applying the direct method of Lyapunov including the determination of a valid Lyapunov function candidate [15]. Analytical means are often impractical if not impossible so a numerical approach is necessary. Through the use of polytopic modeling and linear matrix inequalities the search for possible Lyapunov function candidates can be automated.

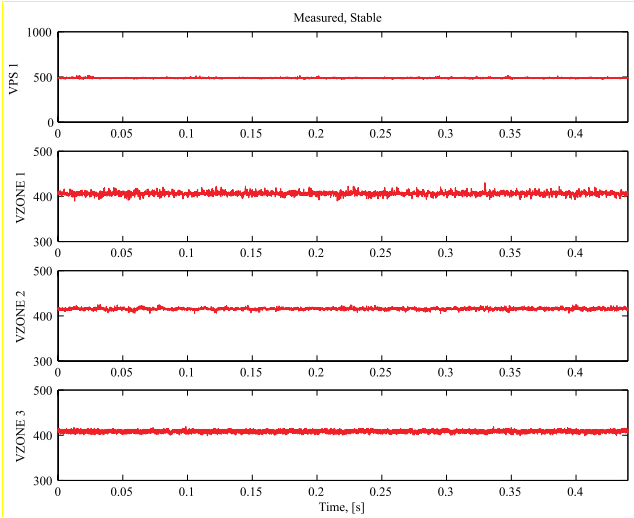

Figure 12. Measured system performance for Case 1.

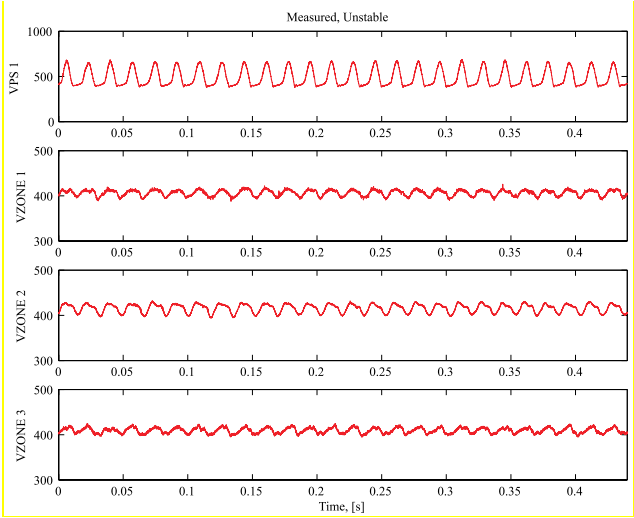

Figure 13 Measured system performance for Case 2.

7.1 Local Models

Local models of the form

$$\dot{\mathbf{x}} = \mathbf{A}\mathbf{x} + \mathbf{B}\mathbf{u} + \boldsymbol{\varphi}_{\mathbf{x}} \tag{4}$$

$$\mathbf{y} = \mathbf{C}\mathbf{x} + \mathbf{D}\mathbf{u} + \boldsymbol{\varphi}_{\mathbf{y}} \tag{5}$$

approximate the behavior of the truth model at a modeling point, $(\mathbf{x}_0, \mathbf{u}_0)$, of interest. The particular characteristics that the local model encapsulates can vary depending on the method used in obtaining the local model. Examples include Taylor series, Teixeira-Żak [16], and the generalized Teixeira-Żak base approximations [17]. All three types of models coincide with the truth model at the operating point. In addition the Teixeira-Żak based model and the Taylor series based model are proportional and coincide, respectively, to the first order behavior at the operating point.

One characteristic of particular interest, but is not forced by the above approximation methods, is having the right hand sides of the local model and the truth model equal one another at the equilibrium pair, $(\mathbf{x}_e, \mathbf{u}_e)$, and the modeling point. Assigning coincident equilibrium pairs can be accomplished by the following procedure.

Step one: form the local model at the modeling point of interest. Step two: perform a coordinate transformation on the local model shifting the desired equilibrium pair to the origin. Step three: perform the generalized Teixeira-Żak based approximation on the shifted local model. Step four: shift the local model back to the original coordinates.

Once the local models have been obtained they are used as ingredients for the polytopic model.

7.2 Polytopic Models

Polytopic models are constructed using a convex combination of local models,

$$\dot{\mathbf{x}} = \sum_{i=1}^{r} \mathrm{w}_i(\boldsymbol{\theta})\left[\mathbf{A}_i\mathbf{x} + \mathbf{B}_i\mathbf{u} + \boldsymbol{\varphi}_{\mathbf{x}i}\right] \tag{6}$$

$$\mathbf{y} = \sum_{i=1}^{r} \mathrm{w}_i(\boldsymbol{\theta})\left[\mathbf{C}_i\mathbf{x} + \mathbf{D}_i\mathbf{u} + \boldsymbol{\varphi}_{\mathbf{y}i}\right]. \tag{7}$$

Thus, (6) and (7) consist of r local models, defined by $\mathbf{A}_i, \mathbf{B}_i, \boldsymbol{\varphi}_{\mathbf{x}i}, \mathbf{C}_i, \mathbf{D}_i, \boldsymbol{\varphi}_{\mathbf{y}i}$, combined by weighting functions, w_i. The weighting functions must satisfy $0 \le \mathrm{w}_i(\boldsymbol{\theta}) \le 1$, $\sum_{i=1}^{r} \mathrm{w}_i(\boldsymbol{\theta}) = 1$, where $\boldsymbol{\theta}$ may be a function of $\mathbf{x}$ or $\mathbf{u}$.

Polytopic models can accurately represent the nonlinear system over a wide range of operation. Although the truth model already has this property the structure of the polytopic model readily lends itself to searching for a Lyapunov function candidate.

7.3 Stability Analysis

Herein it is assumed that all of the local models have coincident equilibrium pairs and the Lyapunov function candidate is of the form

$$V = \tilde{\mathbf{x}}'\mathbf{P}\tilde{\mathbf{x}}, \tag{8}$$

where $\tilde{\mathbf{x}} = \mathbf{x} - \mathbf{x}_e$. Based upon these assumptions the following proposition can be stated.

Proposition 1: If there exists a common $\mathbf{P} = \mathbf{P}' > 0$ such that,

$$\mathbf{A}_i{}'\mathbf{P} + \mathbf{P}\mathbf{A}_i < 0, \quad i = 1,...,r \tag{9}$$

then the equilibrium state satisfying

$$\mathbf{A}_i\mathbf{x}_e + \mathbf{B}_i\mathbf{u}_e + \boldsymbol{\varphi}_i = 0 \quad i = 1,...,r \tag{10}$$

is globally uniformly asymptotically stable (GUAS) in the sense of Lyapunov (ISL) [17].

The search for a matrix $\mathbf{P}$ can be automated by setting up the system of linear matrix inequalities of the form (9) and using commercially available optimization routines. If a common $\mathbf{P}$ is found the polytopic model is GUAS ISL. However stability analysis of the truth model is incomplete.

To complete the stability analysis of the truth model it is necessary to find the region of attraction around the equilibrium state using the direct method of Lyapunov. The region of attraction can be approximated by the largest level set of (8) contained within the region defined by $\dot{V} < 0$, where

$$\dot{V} = 2\tilde{\mathbf{x}}'\mathbf{P}\dot{\tilde{\mathbf{x}}} \tag{11}$$

and $\dot{\tilde{\mathbf{x}}} = \mathbf{F}(\tilde{\mathbf{x}} + \mathbf{x}_e, \tilde{\mathbf{u}} + \mathbf{u}_e)$, where $\tilde{\mathbf{u}} = \mathbf{u} - \mathbf{u}_e$. A Lyapunov function candidate (8) is constructed using $\mathbf{P}$ found in the polytopic model analysis. If a region of attraction is found then the truth model is uniformly asymptotically stabile (UAS) within this region. Research in this area is ongoing. However, the following simple example demonstrates the potential of this analysis technique.

8. POLYTOPIC ANALYSIS EXAMPLE

Consider the second order nonlinear system depicted in Figure 14 and having the parameters listed in Table 5. The source can be viewed as the NLAM of a 3-phase rectifier connected to an infinite bus [4]. The load can be viewed as the NLAM of a converter with a tightly regulated output and a valid operating range limited by the input voltage v_1, [18].

The states of this system are chosen as the inductor current, i_L, and the capacitor voltage, v_C. Local models are obtained using Taylor series approximation at all combinations of $2.5\text{A} < i_L < 50\text{A}$, divided into 19 equally spaced points, and $550\text{V} < v_1 < 650\text{V}$, divided into 20 equally spaced points. The local models are then forced to have coincident equilibrium pairs using the procedure given in the local modeling section. Using linear matrix inequalities (9) formed using the local models a common **P** is found,

$$\mathbf{P} = \begin{bmatrix} 10.16537 & 0.44366 \\ 0.44366 & 1.02148 \end{bmatrix}, \qquad (12)$$

that is symmetric and positive definite. This proves that the polytopic model is GUAS ISL.

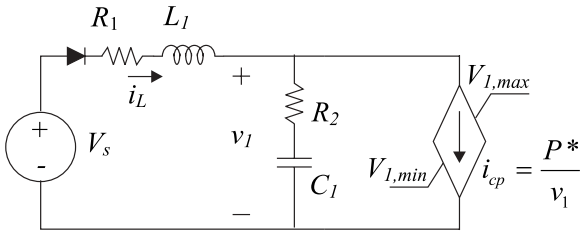

Figure 14. Second order nonlinear system.

Table 5. Second order nonlinear system parameters.

V_s	595.49 V	C_1	1.051 mF
R_1	0.526 Ω	P^*	10 kW
L_1	11.32 mH	V_{1min}	550 V
R_2	0.08305 Ω	V_{1max}	650 V

To analyze the stability of the truth model, (11) is evaluated over a region of the state space surrounding the equilibrium state, see Figure 15. The region in which $\dot{V} > 0$ is shaded black and the operating voltage limits for the load are included as lines. The level set of V satisfying all three constraints forms an ellipse and is included along with one trajectory of the truth model. The ellipse identifies a region of uniform asymptotic stability for the truth model. The trajectory demonstrates the conservative nature of the Lyapunov based analysis.

The previous stability analysis methods discussed in this paper, time domain simulation and generalized immittances, both offer insight into the stability of nonlinear systems. However, neither of the methods identify a region of asymptotic stability about an equilibrium point. Polytopic model structure allows for the automatic search of Lyapunov function candidates, which may be used to search for regions of asymptotic stability as seen in Figure 15. Further research into local model development and the determination of the region of asymptotic stability for higher order systems is on going.

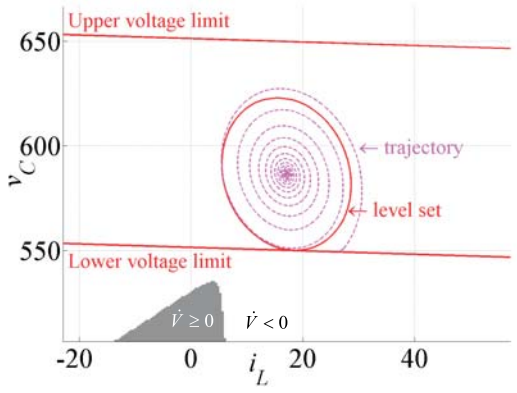

Figure 15. $\dot{V}$ evaluated over the state space.

9. ACKNOWLEDGEMENT

The authors would like to thank the Navy for its support of their efforts. This work was conducted under NAVSEA contract N00024-02-NR-60427 "Naval Combat Survivability" and ONR contract N00014-02-1-0990 "Polytopic Model Based Stability Analysis and Genetic Design of Electric Warship Power Systems."

REFERENCES

[1] Pekarek et. al., A Hardware Power Electronic-Based Distribution and Propulsion Testbed, *Sixth IASTED International Multi-Conference On Power and Energy System*, Marina del Rey, California, May 12-15, 2002.

[2] S.D. Sudhoff, S.D. Pekarek, B.T. Kuhn, S.F. Glover, J. Sauer, D.E. Delisle, Naval Combat Survivability Testbeds for Investigation of Issues in Shipboard Power Electronics Based Power and Propulsion Systems, *Proceedings of the IEEE Power Engineering Society Summer Meeting*, July 21-25, 2002,Chicago, Illinois.

[3] S.D. Pekarek et. al., Development of a Testbed for Design and Evaluation of Power Electronic Based Generation and Distribution System, *SAE2002 Power Systems Conference*, Coral Springs, Florida, October 29-31, 2002.

[4] P.C. Krause, O. Wasynczuk, & S.D. Sudhoff, *Analysis of Electric Machinery*, 2nd ed., John Wiley & Sons, Inc., New York, 2002.

[5] S.H. Żak, *Systems and Control*, Oxford University Press, New York, 2003.

[6] H.K. Khalil, *Nonlinear Systems*, 2nd ed., Prentice Hall, Upper Saddle River, New Jersey, 1996.

[7] www.ESAC.info

[8] S.D. Pekarek, S.D. Sudhoff, J.D. Sauer, D.E.Delisle, E.J. Zivi, "Overview of the Naval Combat

Survivability Program," *Proceedings of the Thirteenth Ship Control Systems Symposium (SCSS 2003)*, Orlando, Florida, April 7-9, 2003.

[9] *MATLAB The Language of Technical Computing*, The MathWorks, Inc., 3 Apple Hill Drive, Natick, MA 01760-2098, 2000.

[10] *Advanced Continuous Simulation Language (ACSL) Reference Manual*, Aegis Simulation, Inc., 6703 Odyssey Drive, Suite 103, Huntsville, AL, 35806, 1999.

[11] S.D. Sudhoff, D.H. Schmucker, R.A. Youngs, H. J. Hegner, Stability Analysis of DC Distribution Systems Using Admittance Space Constraints, *Proceedings of The Institute of Marine Engineers All Electric Ship 98*, London, September 29-30, 1998.

[12] S.D. Sudhoff, S.F. Glover, "Three Dimensional Stability Analysis of DC Power Electronics Based Systems," *Proceedings of the Power Electronics Specialist Conference*, Galway, Ireland, June 19-22, 2000, 101-106.

[13] S.D. Sudhoff, S.F. Glover, P.T. Lamm, D.H. Schmucker, D.E. Delisle, Admittance Space Stability Analysis of Power Electronic Systems, *IEEE Transactions on Aerospace and Electronics Systems*, Vol. 36. No. 3. July 2000, 965-973.

[14] S.D. Sudhoff, S.D. Pekarek, S.F. Glover, S.H. Żak, E. Zivi, J.D. Sauer, D.E Delisle, Stability Analysis of a DC Power Electronics Based Distribution System, *SAE2002 Power Systems Conference*, October 29-31, 2002, Coral Springs, Florida.

[15] H. Lim & D.C. Hamill, Problems of computing Lyapunov exponents in power electronics, *Proceedings of the IEEE International Symposium on Circuits and Systems*, 5, 1999, V-297--V-301.

[16] M.C.M Teixeira & S.H. Żak, Stabilizing controller design for uncertain nonlinear systems using fuzzy models, *IEEE Transactions on Fuzzy Systems*, 7(2), April 1999, 133-142.

[17] S.F. Glover, S.H. Żak, S.D. Sudhoff, and E.J. Zivi, Polytopic modeling and Lyapunov stability analysis of power electronics systems, *Society of Automotive Engineers 2002 Power Systems Conference*, Coral Springs, Florida, October 29-31, 2002.

[18] S.D. Sudhoff, K.A. Corzine, S.F. Glover, H.J. Hegner, & H.N. Robey, DC link stabilized field oriented control of electric propulsion systems, *IEEE Transactions on Energy Conversion*, 13(1), March 1998, 27-33.

Presented at the Thirteenth International Ship Control Systems Symposium (SCSS) in Orlando, Florida, on 7-9 April 2003.